ORDER, DISORDER, AND PHASE TRANSITION IN CONDENSED MEDIA

PHASE TRANSITION AND CROSSOVERS IN THE CAIRO LATTICE OF ISING DIPOLES

© 2024 Yu. A. Shevchenko^{a,b,*}, E. A. Lobanova^{a,b}, I. V. Trefilov^{a,b}, V. S. Strongin^{a,b}, P. A. Ovchinnikov^{a,b}, K. V. Nefedev^{a,b,**}

^aDepartment of Theoretical Physics and Intelligent Technologies, Institute of Science-Intensive Technologies and Advanced Materials, Far Eastern Federal University, Vladivostok, 690922 Russia ^bInstitute of Applied Mathematics, Far Eastern Branch of the Russian Academy of Sciences, Vladivostok 690041, Russia *e-mail: shevchenko.yuriy.a@gmail.com **e-mail: nefedev.kv@dvfu.ru

Received October 31, 2023
Revised July 16, 2024
Accepted July 19, 2024

Abstract. The thermodynamics of finite-number Ising spin systems on the Cairo spin ice lattice is investigated using Monte Carlo numerical calculations in the model of long-range dipole-dipole interaction with limited radius. The Cairo lattice consists of vertices combining three or four nearest neighboring spins. A parameter is added to the model, the variation of which allows changing the balance of interaction energies between vertices with three and four nearest spins without changing the geometry of the Cairo lattice. It is shown that the variational parameter affects the nature of the phase transition process from short-range order to disorder. At low values of this parameter, the transition is a crossover, while at its high values, it is a second-order phase transition.

DOI: 10.31857/S004445102411e087

1. INTRODUCTION

Artificial spin ice is a group of metamaterials consisting of ferromagnetic nanoislands arranged on a non-magnetic substrate in the form of a repeating lattice in such a way that the resulting structure exhibits collective magnetic properties that an individual particle does not possess.

The lattice geometry can impose constraints on configurations, due to which not all pair magnetic interactions between islands can be simultaneously satisfied. This phenomenon is called frustration, and such systems are called frustrated. The first experimentally created structure was square spin ice [1–3], which aimed to simulate the magnetic behavior of the atomic lattice of pyrochlores Dy₂Ti₂O₇ and Ho₂Ti₂O₇ [4] on a plane. It is experimentally easier to observe the magnetization of nanoscale islands on a plane than the spin values in the bulk atomic lattice of a material. Additionally, the possibility emerged to fine-tune the lattice geometry of artificial spin ice and the shape of the island. This

allows selecting convenient experimental values of physical parameters, such as magnetic susceptibility, anisotropy, energy barriers between similar energy configurations, etc. Later, new geometries of two-dimensional spin ices were proposed, which have no analogs among existing naturally occurring materials.

The islands are volumetric objects with fixed height and flat surface. In the plane, XY the island has an oval shape, which leads to shape magnetic anisotropy along the long axis, making the magnetic moment behavior similar to Ising-like. The island is single-domain, and at the same time, the magnetic field induced by neighboring islands is sufficient to change the orientation of the magnetic moment. In experimental works, the geometry and properties of nanoislands are selected to simulate the behavior of the Ising spin. Within the dipolar model, the magnetic state of a nanoisland can be represented as a single-domain nanoscale ferromagnet capable of interacting with other magnetic islands through dipole-dipole exchange. Previously, it was shown that

the point dipole model well describes the behavior of thermally active artificial nanosystems made of permalloy islands, for example, kagome [5], square [6], and Cairo [7] spin ices. Further in the work, the terms "spin," "dipole," and "magnetic moment" (or simply "moment") will be used as synonyms.

Usually in spin ice models, nano-islands lie on the lattice edges. A vertex is defined as a lattice node located at the intersection of edges. It is convenient to consider the magnetic configuration of the system in the context of vertices, specifically the nano-islands adjacent to them. For square spin ice lattice in minimum energy configurations, all vertices follow the ice rule: two macrospins are magnetized towards the vertex, two away from the vertex. A separate class consists of vertexfrustrated lattices [8, 9], in which due to topological constraints it is impossible to make all vertices satisfy the ice rule. As a result, such vertex-unstable structures always contain excitations. These include derivative spin ice structures such as Brickwork [10, 11], Shakti [3, 12, 13], Tetris [14], Santa Fe [15], Saint George and others [16], for example Kagome [3, 17–21] and Cairo [7, 22– 25] (Fig. 1).

Some theoretical works on spin ice consider interactions only between nearest neighbors [13, 17– 19, 26], while for simplification of calculations, longrange energy is assumed to be zero, which is not always justified. Another approach is when authors present vertex interactions in the form of "dumbbell" or "charge" models, which are also short-range. Dipole-dipole interaction depends on the distance r between dipoles and in some cases can lead to long-range ordering [3, 27]. This was shown for three-dimensional tetrahedral pyrochlore lattice [28, 29], where the number of neighbors around a single dipole changes proportionally to r^3 , and the dipolar energy of one pair is proportional to r^{-3} . Thus, the total energy induced by distant neighbors has the same order and can compete with the energy of nearest neighbors. The number of neighbors in a two-dimensional lattice grows much slower, proportionally to r^2 .

2. PHYSICAL MODEL

We consider a system of magnetic moments (point dipoles) on the Cairo lattice [7, 22–25]. The scheme is shown in Fig. 1. The lattice consists of irregular pentagons with four sides of length a and and one side of length b. Two angles of the pentagon are right angles. The lattice has a periodicity parameter

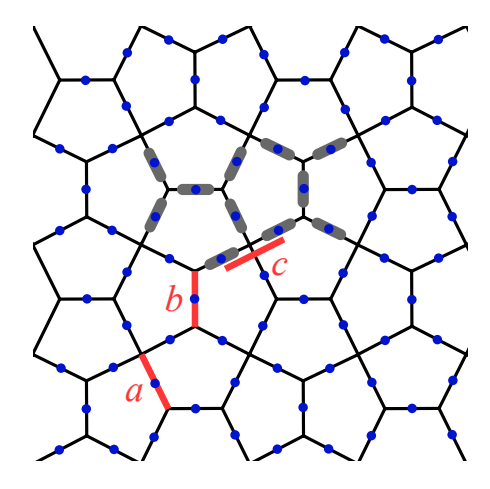


Fig. 1. Schematic representation of the Cairo lattice. Blue dots indicate the location of point dipoles in the studied model, gray ovals show examples of nanoisland placement in corresponding works [7, 30, 31]. Nanoislands are located on all lattice edges; the figure shows only some of them. Red (bold) a, b, c are parameters of the Cairo lattice

 $k = \sqrt{8a^2 - b^2} + b$, which is the same along both axes of the plane XY. The system consists of $N = 20L^2$ identical spins, where L is the linear size, or the number of unit cells along one of the axes. One unit cell consists of 20 spins.

Ferromagnetic nanoislands are located on all lattice edges, one island per edge. The islands have an oval shape and a volume $300 \times 100 \times 2.6 \text{ nm}^3$. The long side of the oval is directed along the lattice edge. The nanoislands are made of permalloy and have no crystallographic axis of anisotropy. In Fig. 1, the nanoislands are shown as gray ovals on several edges as an example.

As shown in [1], the islands are always single-domain due to their small size and large distance between islands. Shape anisotropy ensures magnetization along the long axis. In our model, each nanoisland is considered as a point magnetic dipole, similar to Ising-type, located at the geometric center of the nanoisland. "Similar to Ising-type" means the dipole can only be magnetized along the easy axis of anisotropy of the nanoisland.

Non-equilibrium thermodynamic effects, such as the coercive force of the island and Stoner-Wohlfarth effects [32], are not considered in this work. It is assumed that all relaxation nonequilibrium processes are completed during numerical experiments. Estimates of superparamagnetic transition time are provided in the appendix.

The interaction energy between dipoles i and j is defined as

$$E_{ij,dip} = s_i s_j \left(\frac{(\mathbf{m}_i \cdot \mathbf{m}_j)}{|\mathbf{r}_{ij}|^3} - 3 \frac{(\mathbf{m}_i \cdot \mathbf{r}_{ij})(\mathbf{m}_j \cdot \mathbf{r}_{ij})}{|\mathbf{r}_{ij}|^5} \right), (1)$$

where all vector variables are reduced to unit length, and dimensional coefficients are factored into parameter D of equation (2); \mathbf{m}_i is a unit length moment, whose direction for each dipole is determined by the lattice geometry. The moment has only two possible opposite directions, which are determined by discrete Ising variables $s_i = \pm 1$; \mathbf{r}_{ij} is a radius vector, normalized to the lattice parameter a so that for two points i and j, located at a distance a, from each other, the condition $|\mathbf{r}_{ij}| = 1$ is satisfied.

Similar to [30, 31, 7], this work uses fixed lattice parameters a = 472 nm, b = 344 nm. The Cairo lattice has two types of vertices located at the intersection of three or four edges, forming spin structures of "cross" and "triangle," similar to square and hexagonal spin ice lattices, respectively [27]. This expands the variety of observable phenomena in the considered model. All pair interactions between spins at the lattice site cannot be simultaneously satisfied, leading to frustration effects [3]. The position of islands along edges of length a is determined by parameter c. Increasing c leads to an increase in pair interaction energies in triangular lattice nodes and a decrease in crosses, and vice versa. When c/a = 1, spins are located in the middle of the edge of length a. The position of spins on edge b is always fixed in the middle. In works [30, 31, 7] only parameter c = 376 nm, is considered, although it can vary within 300 nm < c < 644 nm. In extreme cases, the islands will be located close to each other, which can lead to a violation of the symmetry of magnetic configurations, as described in [33]. Here we will consider the influence of parameter c on the thermodynamic characteristics of Cairo dipolar spin ice in the range of values from 376 nm $\approx 0.797a$ to 553 nm ≈ 1.129*a*.

In [30], it was shown that the low-temperature phase transition from long-range order to sublattice order occurs due to dipole-dipole interaction only between pairs of spins directed along vertical or horizontal edges (in the lattice plane) (hereinafter horizontal and vertical spins). Such edges form the base of pentagons and have length b in Fig. 1. These spins are separated from each other by a distance $d = \sqrt{2}k/2 \approx 2.448a$. The nearest horizontally and vertically directed spins do not interact directly with each other, $E_{ij,dip} = 0$. In this work, we do not

consider the energies of pair interactions for which $|\mathbf{r}_{ii}| > d/a$.

A weak vertical magnetic field $\mathbf{H} = \{0, H_y\}$, was added to the model, where $H_y = 1.5 \cdot 10^{-7}$, without which it is impossible to calculate magnetic susceptibility. The system energy is defined as

$$E = D \sum_{[i,j]} E_{ij,dip} - \frac{\mu_0 \mu}{k_B} \sum_i s_i (\mathbf{m}_i \cdot \mathbf{H}), \qquad (2)$$

where the sum [i,j] is taken over all pairs of dipoles separated by a distance not exceeding d. The constant H_y is presented in dimensionless quantities similar to $\mathbf{m}_{y,i}$;

$$D = \mu_0 \mu^2 a^{-3} k_B^{-1}$$

— dimensional coefficient, μ_0 is the magnetic constant, μ — saturation magnetization of the nanoisland, a is the lattice parameter described above, k_B is the Boltzmann constant. All results in this work will be presented in energy units D and length units a. The values presented in units a are rounded to three decimal places. To transition to a dimensional system of calculation, it is necessary to determine the parameters μ and a considering the geometry of the magnetic system.

In our model, periodic boundary conditions along the [01] and [10] axes were used to eliminate boundary effects.

To calculate thermodynamic average values, the canonical single-spin Metropolis algorithm is used [34–36]. Despite its simplicity, it remains a popular method of statistical research in completely different areas of science. For each temperature considered in the work, 10⁵ stabilization Monte Carlo steps and 10⁶ steps were used to calculate thermodynamic averages. Preliminary temperature stabilization of the studied system allows achieving thermodynamic equilibrium at the start of statistics collection. A Monte Carlo step means N Monte Carlo attempts to change the sign of a random s_i . All calculations start from one of the basic states of the lattice. The ground state is understood as such a set of values s_i , at which it is possible to obtain the minimum possible E. At the same time, several configurations of E. The ground state is the most probable at s_i may correspond to the minimum value of $T \rightarrow 0$. System thermalization with increasing T is less demanding on computational resources than with decreasing T.

Ground state configurations for the system under consideration are given in works [30, 31]. All ground states for the long-range model are divided into two groups: with vertically or horizontally directed magnetization vector. The configurations of these groups are separated from each other by an energy barrier that cannot be overcome by the single-spin Metropolis algorithm. In this article, we consider only the group of states with vertical direction of the magnetization vector in the ground state, implying that the behavior of the other group is identical since the lattice is symmetric when rotated by 90°. For the same reason, only a magnetic field directed along the Y axis is added to the model.

3. HEAT CAPACITY OF THE CAIRO LATTICE

Figure 2 shows the heat capacity of the Cairo lattice with N = 9860 dipoles, obtained by the Metropolis method. The heat capacity is obtained as

$$C(T) = \frac{\langle E^2 \rangle - \langle E \rangle^2}{k_B T^2 N}.$$
 (3)

Brackets $\langle ... \rangle$ denote the Gibbs thermodynamic averaging for a given T. The data are shown at c=0.797a, 0.966a, 1.172a with different lines. In this and subsequent figures, points represent values on the abscissa axis for which Monte Carlo calculations were performed. The points are sequentially connected by lines for better visual perception. For heat capacity c=0.797a in the temperature interval 1D < T < 3D the Metropolis algorithm experiences a known critical slowdown problem [37]. This problem is solved by running the algorithm from various random high-energy configurations and averaging heat capacity values between runs in a given temperature range.

The heat capacity has two distinct peaks at temperatures denoted further as T_1 and T_2 . The low-temperature peak $C(T_1)$ does not depend on c. As shown in [30], it is caused exclusively by pair interactions between vertical or horizontal spins separated by distance d, which depends only on lattice parameters a and b, and does not depend on c.

High-temperature maximums of heat capacity occur in the temperature interval 1D < T < 12D. Depending on parameter c, their shape changes from smooth (c = 0.797a) to sharp (c = 1.172a). At medium values (c = 0.966a) the high-temperature

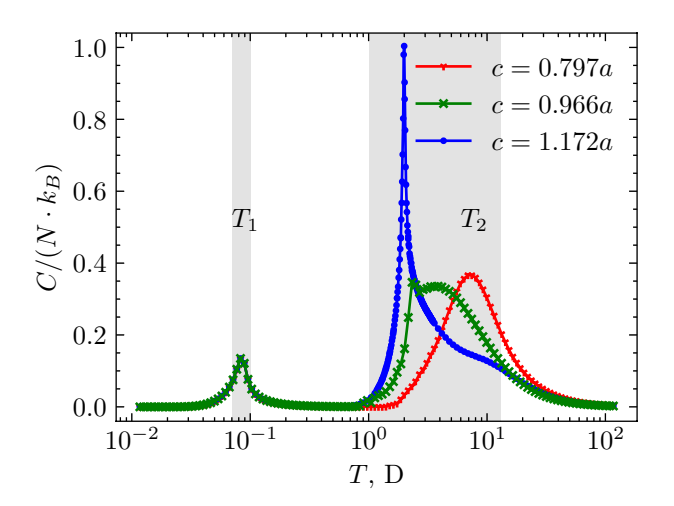


Fig. 2. Heat capacity N=9860 of spins in Cairo spin ice for lattice parameters $c=0.797a,\,0.966a,\,1.172a.$ Gray color marks temperature zones T_1 and T_2 , where heat capacity experiences low-temperature and high-temperature maximums, respectively. The data are calculated using the Metropolis method

peak $C(T_2)$ has two distinct inflections of smooth and sharp form simultaneously. Further, we will examine the reasons for such behavior, show the dependence of height and temperature of the hightemperature peak on parameter c, conduct correlation analysis of configurations in these temperature zones and show the dimensional dependence of height and temperature of both peaks at different c.

4. SIZE EFFECT

According to the classification of phase transitions, including Ehrenfest [38], the discontinuous behavior of statistical sum derivatives indicates the presence of a phase transition at $N \to \infty$. The order of the derivative determines the order of the phase transition. The jump point is the (critical) temperature of phase change. However, there are cases when the phase transition occurs not at a specific temperature point, but in a temperature zone. Known thermodynamic functions do not experience jumps, but this does not mean that such functions do not exist. To denote this effect, we use the generally accepted term crossover (see [39] and § 3.11 in work [40]).

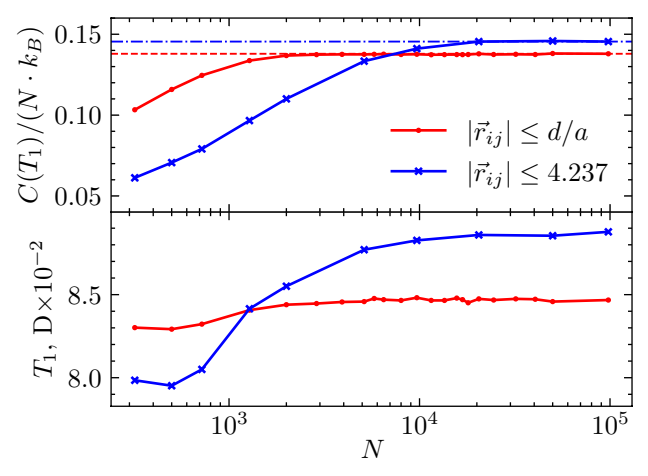
For unambiguous classification and explanation of the heat capacity peaks observed in Fig. 2, it is necessary to consider a model with $N \to \infty$ interacting spins. The solution of such a problem is impossible when using Metropolis algorithms, as they work with finite-size systems. We will examine the change in heat capacity peaks and critical

1.5

1.0

0.5

9.25



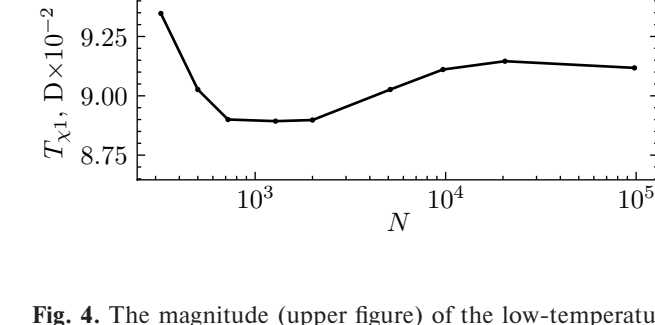


Fig. 3. Values of specific heat (upper figure) and temperature (lower figure) at which the lowtemperature specific heat peak is observed, depending on the number of particles N. The data are presented for the model with maximum interaction radius d (red line with circular points) and the model with radius 4.237a [30] (blue line with crosses). For both models, dashed and dash-dotted lines show the values of specific heat peaks $C(T_1)/N = 0.1379$ and 0.1455 at maximum N respectively

temperatures at different values of N and extrapolate the behavior to $N \to \infty$.

Fig. 3 shows the values of $C(T_1)$ (upper figure) and temperature T_1 (lower figure) at which the lowtemperature specific heat peak has its maximum value, depending on N in the terval of 320 < N < 98000spins. Due to the discrete nature of temperature calculations, the specific heat functions were approximated by a 15th-order curve using the least squares method to obtain the specific heat maximum point with high accuracy. The figure shows data for the model with limited interaction radius $|\mathbf{r}_{ii}| \leq d$ (red line with circular points). For comparison, data from work [30] with increased interaction radius $|\mathbf{r}_{ii}| \le 4.237a$ (blue line with crosses) are added to the figure. In work [30], data are published for N < 9680, for points, an envelope logarithmic function is presented, diverging $N \to \infty$. In this work, due to available computational power, the system size is increased by 10 times and calculation results are presented up to N < 98000.

In this interval, both functions $C(T_1)/N$ reach a plateau, the specific heat at N = 98000 has values of $C(T_1)/N = 0.1379$ and 0.1455 for red and blue lines respectively. These values are marked by dashed and dash-dotted lines in Fig. 3. The behavior of $C(T_1)/N$ for both interaction radii qualitatively coincides. But for $|\mathbf{r}_{ii}| \le d$ the function $C(T_1)/N$ reaches the

Fig. 4. The magnitude (upper figure) of the low-temperature peak of magnetic susceptibility χ and its temperature position (lower figure) depending on the number of particles N

plateau at smaller N, has a lower value and lower temperature T_1 .

Temperature T_1 also reaches a plateau at the same values of N, as $C(T_1)$. As noted in the previous section and in paper [30], the low-temperature peak of heat capacity is caused exclusively by pair interactions between vertical or horizontal spins, whose interaction is similar to the Ising model on a simple square lattice. The variant with $|\mathbf{r}_{ii}| \le d$ is similar to the ferromagnetic Ising model with four nearest neighbors. Variant $|\mathbf{r}_{ii}| \leq 4.237a$ takes into account more distant pairs, not all of which are ferromagnetic. Figure 3 shows that accounting for longer-range interactions increases the length of interspin correlations, affects the absolute value of heat capacity at the critical point and the critical temperature, but generally does not change the nature of the phase transition.

Figure 4 shows the dependence of critical temperatures and values of the low-temperature peak of magnetic susceptibility on N. The susceptibility is defined as

$$\chi(T) = \frac{\langle |\mathbf{m}|^2 \rangle - \langle |\mathbf{m}| \rangle^2}{k_B T N},\tag{4}$$

where the magnetization vector is defined as the sum total vector of all magnetic moments of the system:

$$|\mathbf{m}| = |\sum_{j}^{N} s_{j} \mathbf{m}_{j}|. \tag{5}$$

Example $\chi(T)$ for c = 0.797a was published in paper [30] (Fig. 7). For other values of c considered in this work, the susceptibility $\chi(T)$ has no qualitative differences. The high value of $T_{\chi 1}$ at small N we attribute to the finite size effect, as the low-temperature transition involves 1/5 of all spins in the system [30].

Function $\chi(T_{\chi 1})/N$ versus N also reaches a plateau at N > 9680. However, the peak occurs at higher temperatures than the heat capacity peak. The temperature increase $T_{\chi 1}$ at low values of N is due to the size effect.

Analysis of magnetic configurations in the low-temperature peak region revealed [30] that the peak is caused by the destruction of order between spins located on vertical and horizontal edges of length b. Parameter c does not affect the position of these spins on the lattice edges and does not affect the lattice parameter k. Other spins in the ground state are ordered in such a way that for any horizontal or vertical spin i the condition

$$\sum_{j} E_{ij,dip} = 0,$$

is satisfied, where j only considers spins lying on edges a. The value of any vertical or horizontal spin only affects the energies of pair interactions of similar spins, and this ordering is destroyed at T_1 .

The graph shows $C(T_2)$ (upper figure) and temperature T_2 (lower figure) as a function of N, varying in the interval 320 < N < 98000 spins. Data are presented for lattice parameters c = 0.797a (red line with circular points) and c = 1.172a (blue line

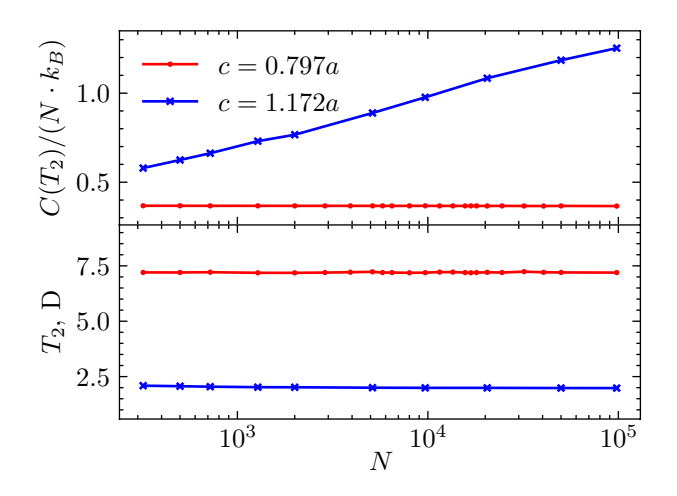


Fig. 5. Heat capacity values (upper figure) and temperature (lower figure) at which the hightemperature heat capacity peak is observed, depending on the number of particles N at lattice parameter c = 0.797a and c = 1.172a

with crosses). In the first case, the heat capacity value at the peak does not depend on N and has a value

$$C(T_2)/N = 0.366 \pm 0.001.$$

In the second case, $C(T_2)/N$ has a logarithmic dependence on N, and in the limit as $N \to \infty$ may diverge.

5. LATTICE PARAMETER EFFECT

As described above, parameter c affects the distance between two nearest collinear spins. Increasing c leads to increased pair interaction energies in triangular lattice nodes and decreased energies in crosses. The destruction of magnetic order within crosses and triangles itself requires energy expenditure and should lead to two heat capacity peaks at temperatures proportional to pair interaction energies within crosses and triangles respectively.

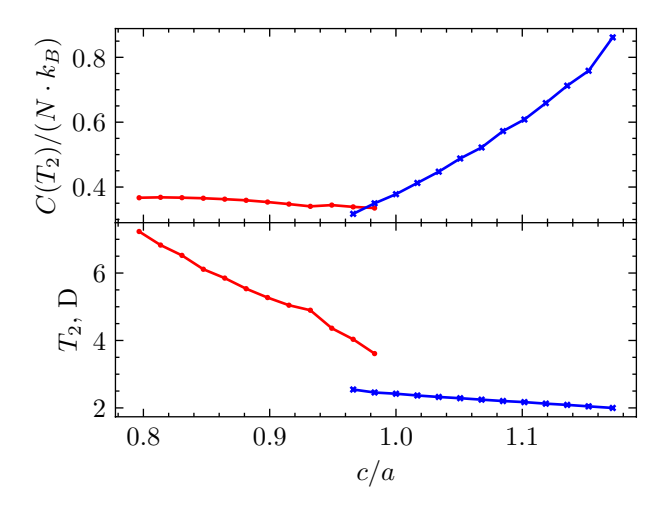
As shown in Fig. 2, at low values of c the heat capacity has one smooth high-temperature peak. As c increases, upon reaching a critical value of approximately 0.966a (456 nm), a second sharp high-temperature peak appears in the heat capacity, which is visible on the green shown by the blue line with crosses in Fig. 2. With further increase in c, the height of the sharp peak increases, and the smooth peak decreases until it becomes impossible to definitively identify.

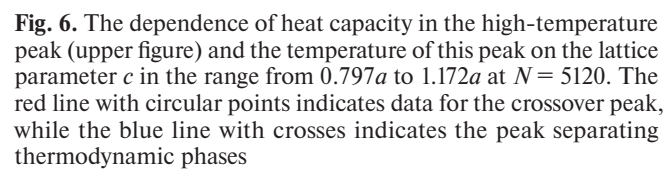
Fig. 6 shows the heat capacity values and temperatures of the two described high-temperature peaks. The lines are marked with different colors, and in the region of c = 0.966a two peaks are present simultaneously.

Let's introduce a correlation parameter that only accounts for the sign of the pair interaction energy, whose absolute value does not depend on parameter *c*:

$$G = \sum_{[i,j]} \frac{E_{i,j}}{|E_{i,j}|} / n. \tag{6}$$

The sum [i,j] only considers unique pair interactions that require correlation analysis, n is the number of such pairs. Let's define that parameter G_t only accounts for pair interactions in all triangles. There is no triangle configuration where all pair interactions will be $E_{ij} < 0$. In the minimum energy configuration, two pairs will have $E_{ij} < 0$ and one pair will have $E_{ij} > 0$. In the maximum energy configuration, all three pairs will have $E_{ij} > 0$. The





values of parameter G_t for a single triangle will vary from -1/3 in the minimum energy configuration to 1 in the maximum energy configuration.

Defined similarly to G_t parameter G_k considers only nearest-neighbor pair interactions in all crosses separated by distanc $\sqrt{2}c$. For a cross, it is possible to create a configuration where all four pair interactions will be with $E_{ij} < 0$, therefore the parameter values G_k for an individual cross will vary from -1 in the minimum energy configuration to 1 in the maximum energy configuration.

Figure 7 shows the Gibbs thermodynamically averaged parameters G_t (upper half) and G_k (lower half) as a function of temperature for lattice parameters $c=0.797a,\,0.966a,\,1.172a$ and N=5120 spins. Data is presented for temperatures at which the heat capacity experiences a high-temperature peak. The change in value G(T) indicates the influence of the corresponding temperature on the magnetic ordering of crosses or triangles.

For parameter c = 0.797a the correlation level in triangles and crosses decreases at temperatures close to each other. Since all spins lying on edges of length a, are simultaneously present in both triangles and crosses, random temperature fluctuations of individual lattice spins lead to the disappearance of magnetic ordering simultaneously in crosses and triangles adjacent to these spins, as the energies of nearest-neighbor interactions in crosses and triangles

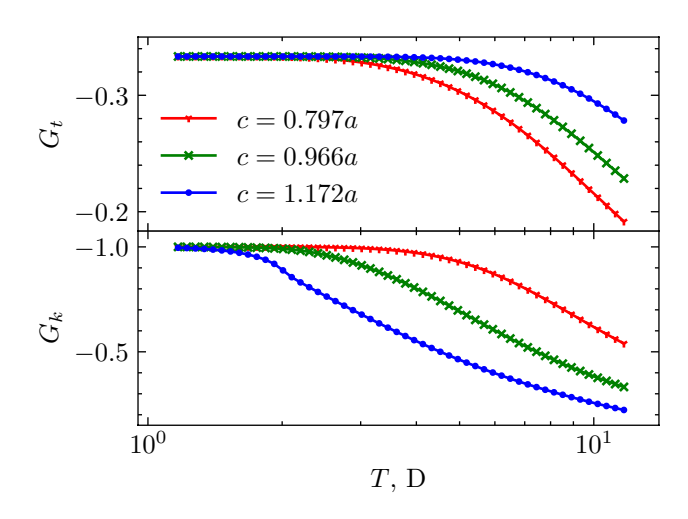


Fig. 7. Temperature dependence of correlations within triangles G_t and crosses G_k for lattice parameters c = 0.797a, 0.966a, 1.172a and N = 5120 spins

are approximately equal in magnitude. Such behavior corresponds to the definition of a crossover, where the phase change from frozen order to disorder occurs over a temperature zone rather than at a specific temperature point.

As parameter c decreases, the distance between the spins of triangles decreases, which results in an increase in the magnitude of pair interaction energies within triangles, leading to an increase in the temperature required to destroy the order. On the other hand, increasing parameter c leads to an increase in the distance between cross spins. As a result, when c increases, the inflection temperature G_t rises, while G_k decreases. At parameter c = 1.172athe temperature difference becomes significant. Parameter G_k for c = 1.172a experiences an inflection in the region of the high-temperature heat capacity peak from Fig. 2. In this temperature range, parameter G_t takes the minimum possible value. This means that magnetic ordering disappears in crosses but persists in all triangles. This can only be achieved if temperature fluctuations lead to remagnetization of the entire triangle instead of a single dipole. Triangle remagnetization has a higher energy barrier compared to remagnetization of a single dipole. This results in the sharp nature of the high-temperature peak in Fig. 2.

Let's note how parameter c affects the pair energy interactions between triangle spins. The decrease of c moves two of the three spins along the lattice edge of length a. The third spin of the triangle remains in place, so the pair interaction energies in the triangle

change in different proportions. The triangle angles are not equal to each other. Pair interactions within the triangle break down at different temperatures, therefore the drop in $G_t(T)$ in Fig. 7 does not lead to a sharp heat capacity peak at the corresponding temperature. Unlike the triangle, the cross edges are positioned at right angles to each other, the parameter c equally affects all cross spins, all four pair interaction energies within the cross are equal in magnitude. This further explains the sharp nature of the corresponding heat capacity peak.

6. CONCLUSIONS

We investigated the temperature behavior of the heat capacity in a model of Ising-like dipoles on the Cairo lattice. According to Ehrenfest's universal classification, a second-order phase transition is accompanied by divergence of second derivatives of internal system parameters as the number of particles in the system approaches infinity. For the considered finite-size lattice, two heat capacity peaks are observed when conducting numerical experiments using the Metropolis algorithm. In work [30], it was shown that the low-temperature heat capacity peak has no tendency to diverge and is solely caused by the order-disorder transition between spins connected only by long-range dipole-dipole interaction. In other words, the low-temperature peak is caused by the disappearance/emergence of long-range ordering.

According to the classification of phase transitions (see §3 in work [41]), systems of the same universality class possess a similar set of phases, and the phase change process can be described by universal critical exponents. The universality class of our system is determined by two parameters: the space dimension and the number of degrees of freedom of a single spin. We showed that the lattice parameter c, which does not determine the universality class, can change the nature of the phase transition in this classification while other system parameters remain unchanged.

At a low value of the parameter c the system undergoes a "phase" transition, where shortrange magnetic ordering within crosses and triangles disappears in a temperature zone rather than at a specific critical temperature. This leads to the absence of heat capacity singularity across the entire temperature interval at $N \to \infty$, and such transition is called a crossover [39, 40]. A similar effect occurs, for example, in ultracold Fermi gases, where the system transitions from a Bose-Einstein condensate

state to a Bardeen-Cooper-Schrieffer state as the interaction strength changes [42]. Another example is magnetic alloys with magnetic impurities, where the Kondo effect is studied [43], where a normal Fermi liquid phase (weakly coupled to impurities) transitions to a "local" Fermi liquid phase, in which conduction electrons form strongly bound spinsinglets with impurity electrons, without an explicit phase transition.

At a high value of the parameter c the system undergoes a phase transition "short-range order-disorder" in the high-temperature zone. It is characterized by heat capacity divergence at a specific temperature point at $N \to \infty$ and is caused by the disappearance of order in the crosses.

Thus, we have demonstrated the existence of a magnetic system where changing a single lattice parameter leads to a qualitative change in its thermodynamic behavior

ACKNOWLEDGMENTS

The authors express their gratitude to the management of the Institute of High Technologies and Advanced Materials of FEFU for their invaluable contribution to the "development" of supercomputing in the Far East.

FUNDING

The results presented in this work were obtained using the supercomputer cluster of the Institute of Applied Mathematics, FEB RAS. The study was funded by the Russian Science Foundation grant No. 23-22-00328, https://rscf.ru/project/23-22-00328/.

APPENDIX

To prove the possibility of experimental reproduction of the effects shown in this work, we will demonstrate that the average relaxation time of a nanoparticle with the considered geometry is within typical experimental observation limits. The magnetic relaxation time τ of a superparamagnet follows the Neel-Arrhenius law

$$\tau^{-1} = f_0 \exp(-\Delta U / k_B T), \tag{7}$$

where k_B is the Boltzmann constant, T is temperature, ΔU , f_0 is the pre-exponential factor or frequency factor, which for permalloy nanoparticles is $10^{12} \, \mathrm{s}^{-1}$

[44, 5, 45]. Ising-like behavior of the nanoparticle is achieved through shape anisotropy in the absence of other magnetic anisotropy sources (permalloy).

Let's consider the relaxation time of an individual nanoparticle without external field influence. Then $\Delta U = KV$, where V is the particle volume, K is the magnetic anisotropy energy density. Shape anisotropy along the $d \in \{x,y,z\}$ axis is defined as [46]

$$K_d = \frac{1}{2} \mu_0 \, N_d \, M^2,$$

where μ_0 is the magnetic constant, M is the residual magnetization of the material, N is the demagnetizing factor.

At room temperature T = 290 K for bulk permalloy M = 800 kA/m [7], but for a film with thickness of 2.6 nm M = 100 kA/m [5].

The method for determining N_d is presented in work [47] for ellipsoids and refined in [48] for prisms. $N_d = 0.14036$ along the direction of the long side of the prism.

The magnitude of the energy barrier caused by shape anisotropy without the influence of other forces will be $\Delta U = 6.87 \cdot 10^{-20}$ J, or 0.43 eV, which corresponds to $\tau = 2.89 \cdot 10^{-5}$ s.

Let's consider the average energy of dipole-dipole interaction from Monte Carlo simulation results:

$$\Delta U = KV + \langle E \rangle / N,$$

where E is defined by formula (2), and the value of $\langle E \rangle$ is taken in absolute terms. We obtain $\langle E \rangle/N = 8.09 \cdot 10^{-21}$ J, or 0.05 eV, which corresponds to $\tau = 2.18 \cdot 10^{-4}$ s.

With decreasing T the M permalloy increases and, consequently, ΔU , increases, which will lead to a rapid increase in τ . Estimating the dependence of M on T for a nanoparticle is the subject of additional research and is beyond the scope of this article. For example, at T=250 K and M=120 kA/m we obtain $\tau=38$ s.

The presented estimates are in the order of seconds and correspond to the experiment [49](Fig. 4b).

REFERENCES

1. R.F. Wang, C. Nisoli, R.S. Freitas et al., Nature **439**, 303 (2006).

- 2. C. Nisoli, R. Moessner, P. Schiffer, Rev. Mod. Phys. 85, 1473 (2013)
- Y. Shevchenko, A. Makarov, and K. Nefedev, Phys. Lett. A 381, 428 (2017).
- **4.** *Y. Shevchenko, K. Nefedev, and Y. Okabe*, Phys. Rev. E **95**, 052132 (2017).
- **5.** *A. Farhan, P. M. Derlet, A. Kleibert et al.*, Nature Phys. **9**, 375 (2013).
- **6.** *A. Han, P. M. Derlet, A. Kleibert et al.*, Phys. Rev. Lett. **111**, 057204 (2013).
- 7. *M. Saccone, K. Hofhuis, Y. Huang et al.*, Phys. Rev. Mater. **3**, 104402 (2019).
- **8.** *M. J. Morrison, T. R. Nelson, and C. Nisoli*, New J. Phys. **15**, 045009 (2013).
- **9.** *S.H. Skjærvø*, *C.H. Marrows*, *R.L. Stamps et al.*, Nat. Rev. Phys. **2**, 13 (2020).
- **10.** *J. Park, B.L. Le, J. Sklenar et al.*, Phys. Rev. B **96**, 024436 (2017).
- **11.** *Y. Li, T.X. Wang, Z.T. Hou et al.*, Phys. Lett. A **380**, 2013 (2016).
- **12.** *G.W. Chern, M.J. Morrison, and C. Nisoli*, Phys. Rev. Lett. **111**, 177201 (2013).
- **13.** *I. Gilbert, G.W. Chern, S. Zhang et al.*, Nature Phys. **10**, 670 (2014).
- **14.** *I. Gilbert, Y. Lao, I. Carrasquillo et al.*, Nature Phys. **12**, 162 (2015).
- **15.** X. Zhang, A. Duzgun, Y. Lao et al., Nature Communications **12**, (2021).
- **16.** *H. Stopfel, U.B. Arnalds, A. Stein et al.*, Phys. Rev. Mater. **5**, 114410 (2021).
- **17.** *G.W. Chern, P. Mellado, and O. Tchernyshyov*, Phys. Rev. Lett. **106**, 207202 (2011).
- **18.** *G.W. Chern and O. Tchernyshyov*, Phil. Trans. Royal Soc. A: Math., Phys. Engin. Sci. **370**, 5718 (2012).
- **19.** *G. Möller and R. Moessner*, Phys. Rev. B **80**, 140409 (2009).
- **20.** A.G. Makarov, K. Makarova, Y.A. Shevchenko et al., JETP Lett. **110**, 702 (2019).
- **21.** *U.B. Arnalds, A. Farhan, R.V. Chopdekar et al.*, Appl. Phys. Lett. **101**, 112404 (2012).
- 22. I. Rousochatzakis, A.M. Läuchli, and R. Moessner, Phys. Rev. B 85, 104415 (2012).
- **23.** *A.M. Abakumov, D. Batuk, A.A. Tsirlin et al.*, Phys. Rev. B **87**, 024423 (2013).
- **24.** *M. Rojas, O. Rojas, and S.M. Souza*, Phys.Rev.E **86**, 051116 (2012).
- **25.** A.A. Tsirlin, I. Rousochatzakis, D. Filimonov et al., Phys. Rev. B **96**, 094420 (2017).
- **26.** *C. Castelnovo, R. Moessner, and S. L. Sondhi*, Nature **451**, 42 (2008).
- **27.** Y.A. Shevchenko, A.G. Makarov, P.D. Andryushchenko et al., JETP **151**, 1146 (2017).

- **28.** *R.G. Melko, B.C. Hertog, and M.J.P. Gingras*, Phys. Rev. Lett. **87**, 067203 (2001).
- **29.** *R.G. Melko and M.J.P. Gingras*, J. Phys.: Cond. Matt. **16**, 1277 (2004).
- **30.** *Y. Shevchenko, V. Strongin, V. Kapitan et al.*, Phys. Rev. E **106**, 064105 (2022).
- **31.** *K. Makarova, V. Strongin, I. Titovets et al.*, Phys. Rev. E **103**, 042129 (2021).
- **32.** *E.C. Stoner and E.P. Wohlfarth*, Phil. Trans. Royal Soc. London. Series A, Math. Phys. Sci. **240**, 599 (1948).
- **33.** *S. Gliga, A. Kákay, L.J. Heyderman et al.*, Phys. Rev. B **92**, 060413 (2015).
- **34.** N. Metropolis, A. W. Rosenbluth, M.N. Rosenbluth et al., J. Chem. Phys. **21**, 1087 (1953).
- **35.** W.K. Astings, Biometrika **57**, 97 (1970).
- **36.** *K. Makarova, A. Makarov, V. Strongin et al.*, J. Comp. Appl. Math. **427**, 115153 (2023).
- **37.** *H. Gould and J. Tobochnik*, Comp. Phys. **3**, 82 (1989).
- **38.** A.A. Gukhman, Foundations of Thermodynamics, LKI (2010).

- **39.** *S. Gluzman and V.I. Yukalov*, Phys. Rev. E **58**, 4197 (1998).
- **40.** H. Nishimori and G. Ortiz, Elements of Phase Transitions and Critical Phenomena, Oxford University Press (2010).
- **41.** *C.A.F. Vaz, J.A.C. Bland, and G. Lauhoff*, Rep. Prog. Phys. **71** 056501 (2008).
- **42.** *T. Bourdel, L. Khaykovich, J. Cubizolles et al.*, Phys. Rev. Lett. **93**, 050401 (2004).
- **43.** *W.G. Van der Wiel, S.D. Franceschi, T. Fujisawa et al.*, Science **289**, 2105 (2000).
- **44.** *P. Lubitz, M. Rubinstein, JJ. Krebs et al.*, J. Appl. Phys. **11**, 6901 (2001).
- **45.** *A. Farhan, A. Scholl, C. Petersen et al.*, Nature Commun. **1**, 12635 (2016).
- **46.** W.F. Brown Jr. and A.H. Morrish, Phys. Rev. **4**, 1198 (1957).
- 47. J.A. Osborn, Phys. Rev. 11-12, 351 (1945).
- **48.** A. Aharoni, J. Appl. Phys. **6**, 3432 (1998).
- **49.** *M. Saccone, A. Scholl, S. Velten et al.*, Phys. Rev. B **22**, 224403 (2019).